CityU Scholars

Camel-Fur-Inspired Graphite-Based Hygroscopic Membrane for Passive Air Cooling with Ultrahigh Cooling Power

Lin, Wenzhu; Yao, Xiaoxue; Nallapaneni, Manoj Kumar; Lo, Wai Kin; Chopra, Shauhrat S.; Ng, Yun Hau; Wang, Steven

Published in:
Advanced Energy Materials

Published: 26/04/2024

Document Version:
Final Published version, also known as Publisher's PDF, Publisher's Final version or Version of Record

License:
CC BY-NC-ND

Publication record in CityU Scholars:
Go to record

Published version (DOI):
10.1002/aenm.202303470

Publication details:
Lin, W., Yao, X., Nallapaneni, M. K., Lo, W. K., Chopra, S. S., Ng, Y. H., & Wang, S. (2024). Camel-Fur-Inspired Graphite-Based Hygroscopic Membrane for Passive Air Cooling with Ultrahigh Cooling Power. *Advanced Energy Materials*, *14*(16), Article 2303470. https://doi.org/10.1002/aenm.202303470

Citing this paper
Please note that where the full-text provided on CityU Scholars is the Post-print version (also known as Accepted Author Manuscript, Peer-reviewed or Author Final version), it may differ from the Final Published version. When citing, ensure that you check and use the publisher's definitive version for pagination and other details.

General rights
Copyright for the publications made accessible via the CityU Scholars portal is retained by the author(s) and/or other copyright owners and it is a condition of accessing these publications that users recognise and abide by the legal requirements associated with these rights. Users may not further distribute the material or use it for any profit-making activity or commercial gain.

Publisher permission
Permission for previously published items are in accordance with publisher's copyright policies sourced from the SHERPA RoMEO database. Links to full text versions (either Published or Post-print) are only available if corresponding publishers allow open access.

Take down policy
Contact lbscholars@cityu.edu.hk if you believe that this document breaches copyright and provide us with details. We will remove access to the work immediately and investigate your claim.

Download date: 18/04/2025

Check for updates

ADVANCED ENERGY MATERIALS
www.advenergymat.de

Camel-Fur-Inspired Graphite-Based Hygroscopic Membrane for Passive Air Cooling with Ultrahigh Cooling Power

*Wenzhu Lin, Xiaoxue Yao, Nallapaneni Manoj Kumar, Wai Kin Lo, Shauhrat S. Chopra, Ng Yun Hau, and Steven Wang**

Earth's temperature has risen by ≈0.18 °C per decade since 1981 and year 2022 is the sixth-warmest year on record. The exploration of cooling strategies that operate with less energy consumption is thus highly desirable. Through this project, a camel-fur-inspired passive membrane encapsulated sorbent cooler that can periodically absorb moisture from the atmosphere and release it for daytime evaporative cooling, leading to effective regulation of building temperature without additional energy input is demonstrated. This sorbent cooler with high sorption capacity is made of anhydrous salt and modified expanded graphite and further encapsulated by a breathable porous membrane. This novel material is shape-stabilized, and it has excellent cycling performance, and remarkable water adhesion ability. In this evaporative-cooling demonstration, the average cooling power of the camel-fur-inspired sorbent can reach up to 630 W m^{-2}, which is much higher than the radiative cooling approach. This theoretical model implies that the proposed sorbent cooler has the potential to cut down cooling energy carbon emission by 61% to 87.83% when compared to emissions released from cooling energy usage in reference buildings. This nature-inspired approach paves a new way for efficient space cooling without extra water supply and with minimized energy consumption.

1. Introduction

As the Earth's temperature rises, cooling has become an essential aspect of our daily lives, especially in space cooling.[1] Space cooling accounts for almost 40% of primary building energy usage,[2,3] and the global demand is predicted to rise due to the occurrence of extreme heat events and higher living standards.[4–6] Air compression-based air conditioners are the most used refrigeration devices for residential and industrial cooling. However, these devices consume a significant amount of energy and contribute to severe environmental pollution in carbon dioxide (CO_2) equivalents.[7] Energy shortages are becoming more frequent, particularly in impoverished regions.[8,9] Thus, it is vital to develop cooling technologies that consume less energy to improve the quality of life in relatively energy-poor areas.

Semi-passive and passive cooling methods are becoming popular due to their high efficiency and energy savings, unlike electricity-driven vapor compression systems. One such method is radiative cooling, where a body emits heat to the universe through thermal radiation without any extra input energy. This process utilizes the transparent window between 8–13 um of the universe, which acts as a heat sink with absolute zero temperature.[10–12] However, radiative cooling is limited due to the low solar reflectivity and emissivity of radiative materials, resulting in less than 160 W m^{-2} cooling power. Moreover, high humidity in ambient climates absorbs infrared radiation, rendering the transparent window ineffective.[13–15] In contrast, thermal sorption is a flexible and stable cooling method that relies on the transfer of heat between different substrate materials.[16,17]

W. Lin, X. Yao, W. K. Lo, S. Wang
Department of Mechanical Engineering
City University of Hong Kong
Kowloon, Hong Kong 999077, China
E-mail: steven.wang@cityu.edu.hk

The ORCID identification number(s) for the author(s) of this article can be found under https://doi.org/10.1002/aenm.202303470

© 2024 The Authors. Advanced Energy Materials published by Wiley-VCH GmbH. This is an open access article under the terms of the Creative Commons Attribution-NonCommercial-NoDerivs License, which permits use and distribution in any medium, provided the original work is properly cited, the use is non-commercial and no modifications or adaptations are made.

DOI: 10.1002/aenm.202303470

W. Lin, X. Yao, W. K. Lo, S. Wang
Centre for Nature-Inspired Engineering
City University of Hong Kong
Kowloon, Hong Kong 999077, China

N. M. Kumar, S. S. Chopra, N. Y. Hau, S. Wang
School of Energy and Environment
City University of Hong Kong
Kowloon, Hong Kong 999077, China

N. M. Kumar
Centre for Circular Supplies
HICCER – Hariterde International Council of Circular Economy Research
Palakkad, Kerala 678631, India

Materials including NH_3NO_3, NH_4Cl_2, $LiBr/H_2O$, NH_3/H_2O, $LiCl/H_2O$, and $CaCl_2/H_2O$ store and release heat in a reversible endothermic/exothermic process.[18–20] Evaporative cooling is another energy-saving, proven to be environment-friendly when compared to radiative cooling, and an easy-to-maintain technique that lowers temperatures through the phase transition of a liquid to vapor.[19] However, this method usually requires an adequate water supply, which can be a challenge in impoverished regions facing severe water scarcity throughout the year.[21]

Considering the above-highlighted challenge of evaporative cooling, a nature-inspired approach that requires zero water requirements was proposed. Inspired by the cooling strategy of camels in the desert, we demonstrate a passive sorbent cooling cooler that can absorb moisture from the air and subsequently release it during the day to achieve cooling. As liquid water evaporates, a vast amount of heat is extracted, leading to a temperature drop in the environment. As a proof of concept, we proposed encapsulated a super-hydrophilic matrix containing hygroscopic salt in an innovative porous membrane to create a sorbent cooler. Anhydrous salt LiCl, was used as the sorbent due to its excellent water sorption for a wide range of RH, exceptional chemical stability, and low cost.[22,23] The super-hydrophilic expanded graphite matrix offers abundant water sorption pores and salt adhesion sites, improving its stability and cycling performance. The breathable polytetrafluoroethylene (PTFE) membrane enables airflow while avoiding water leaks.[24] The sorbent could absorb the atmospheric water vapor at night and release moisture during the day for evaporative cooling. Simultaneously, leak-free character not only avoids the carryover of liquid sorbent with the air, but also prevents the corrosive performance of sorbent to the channels, thus ensuring the cycling performance of the evaporative cooler. This novel porous membrane-encapsulated sorbent we proposed is an advanced material that can offer an easily accessible, equitable, and eco-friendly solution for indoor temperature reduction without additional water consumption. Hence, we conduct this study to experimentally reveal the potential of camel-fur-inspired graphite-based hygroscopic membrane for passive air cooling by first testing on a laboratory prototype building in terms water sorption performance, performance of the membrane encapsulated LiCl/SHEG, and cooling performance; then leveraging it to experience various climate conditions through extensive simulations following ASHRAE standards for informed decisions on how well this cooling technology would perform both in terms of cooling energy saving and carbon mitigation potential.

2. Results and Discussion

2.1. Working Principle

The camel's remarkable adaptations to extreme changes in temperature are well-known. To cope with fluctuating thermal environments, the camel stores a considerable amount of water in the blood vessels beneath its fur. The water is then released through sweat glands spread throughout the skin to regulate its body temperature (as shown in **Figure 1A**). Inspired by this natural process, we have created a sorbent cooler that can absorb moisture from the air during the night and release it during the day to achieve cooling (as depicted in Figure 1B). The significant latent heat conversion achieves this cooling effect during the liquid-to-gas phase transition. As illustrated in Figure 1C, the sorbent absorbs atmospheric water; this absorbed water evaporates from the wetted sorbent absorbing heat and causing the air to leave the sorbent at a lower temperature. It is worth noting that constant airflow is required to facilitate the entire process; but the driving power of the constant airflow is much lower than the achieved cooling power, thus it can be considered passive (as evidenced in references).[25,26] The high concentration of salt particles in the sorbent at night leads to a relatively low vapor pressure within the sorbent, allowing it to quickly absorb moisture from the surrounding air.[27] The resulting cooling power can be calculated as follows:

$$P = \frac{H \times \Delta m}{t \times S} \quad (1)$$

where H is the latent heat of vaporization of the liquid being evaporated, Δm is the weight loss of sorbent room due to the water evaporation, t is the test time and S is the surface area of indoor room.

The sorbent material chosen was the anhydrous salt LiCl due to its excellent water sorption ability.[28] However, hydrous salts can encounter issues such as solution carryover, swelling, and agglomeration,[29] which pose a significant risk of harm to people inhaling the air. To tackle these problems, a porous matrix and a breathable but waterproof membrane were selected (as shown in Figure 1C). Impregnating hygroscopic salts into porous materials can improve their water sorption characteristics while maintaining shape stability and enhancing heat and mass transfer ability.[24,30,31] Porous matrices typically have large pore volumes, high specific surface areas, and appropriate pore sizes that provide mass transfer channels and load hygroscopic salts. Expanded graphite (EG) is widely used in salt sorption,[32,33] due to its porosity that enhances sorption kinetics, but its poor hydrophilicity,[34] may result in water leakage, especially during salt deliquescence.[35] Hydrophilic modification can greatly alleviate leakage problems,[36] and in this study, a hydrophilic modified expanded graphite with super hydrophilicity was proposed to improve water adhesion of the salt and alleviate agglomeration issues. Additionally, the sorbent was encapsulated with a porous PTFE membrane that is moisture permeable but waterproof, allowing airflow while preventing water leaks. As a result, the salt solution can be confined within the membrane, avoiding the risk of solution leakage and carryover, preventing the corrosive properties of the salt, and ensuring the sorbent's cycling performance.[24]

A comprehensive comparison was conducted to assess the cooling performance of a novel sorbent cooler inspired by camel fur, as shown in Figure 1D.[37–47] This study compared the cooling method with other methods previously investigated in the literature, namely radiative cooling (RA), evaporative cooling (EVA) based on atmospheric water harvesting (similar to the method used in this study), and the combined method of radiative cooling and evaporative cooling (RA+EVA) (refer to Supporting Note 1 for more details). The figure clearly demonstrates that the cooling power of the novel sorbent cooler outperforms radiative cooling in all circumstances. Furthermore, when compared to evaporative cooling based on atmospheric water harvesting,

© 2024 The Authors. Advanced Energy Materials published by Wiley-VCH GmbH

16146840, 2024, 16, Downloaded from https://onlinelibrary.wiley.com/doi/10.1002/aenm.202303470, Wiley Online Library on [15/07/2024]. See the Terms and Conditions (https://onlinelibrary.wiley.com/terms-and-conditions) on Wiley Online Library for rules of use; OA articles are governed by the applicable Creative Commons License

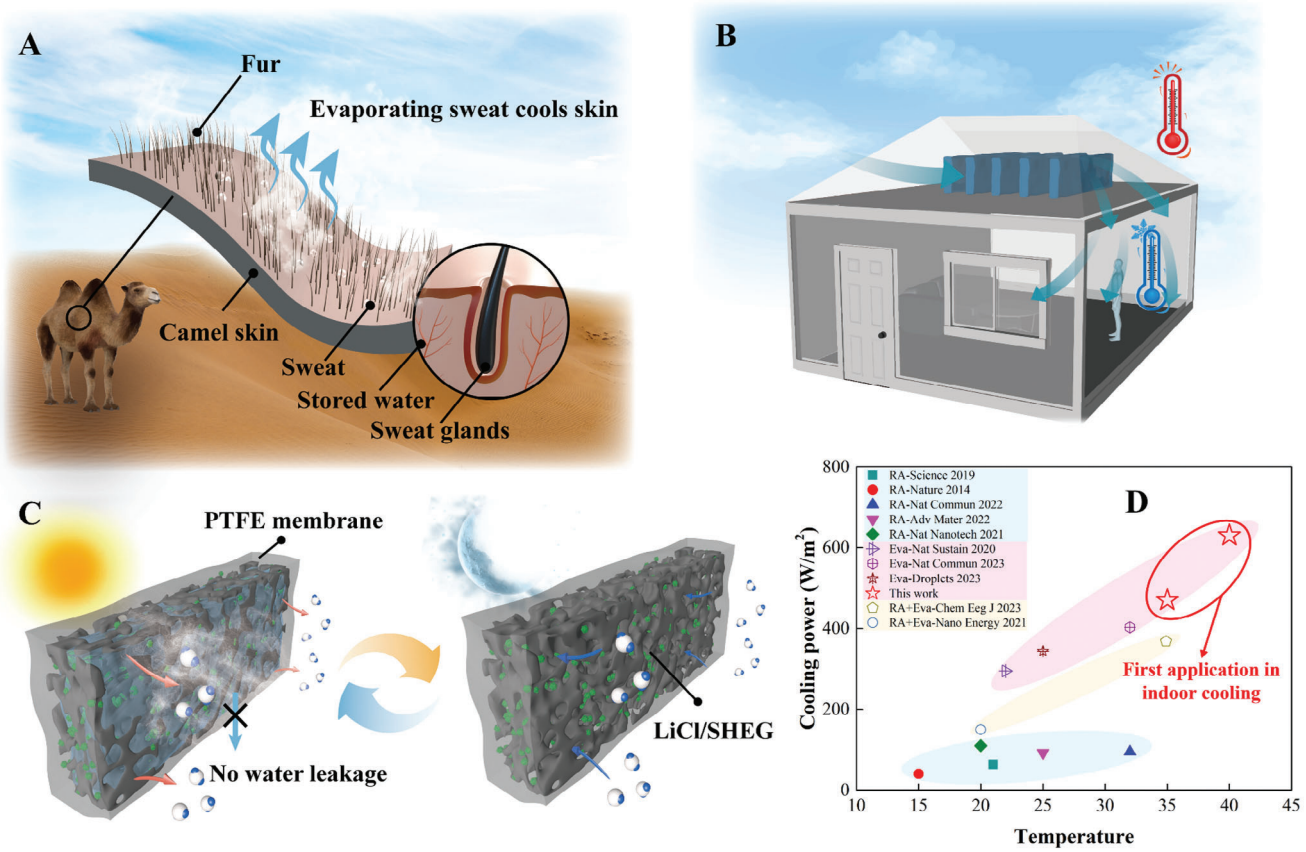

Figure 1. Camel-fur-inspired graphite-based passive sorbent cooling. A) Schematic of the evaporative cooling of camel. B) Schematic illustration of the sorbent supplying cold air to the indoor room. C) Working principle of the sorbent cooling system. D) Cooling power comparisons of this work and previously reported methods.[37–47]

the cooling power achieved in this study demonstrates superior performance, particularly under higher temperature conditions.

Overall, this emerging passive approach can provide effective indoor temperature regulation based on the atmosphere water harvesting (AWH) and evaporative cooling (EVA), which does not need to expose to the sun to achieve effective cooling (compared with radiative cooling).

2.2. Synthesis and Characterization LiCl/SHEG

We modified the expanded graphite by making it hydrophilic through a super hydrophilic modification. To achieve this, we dispersed the expanded graphite with the surfactant TritonX-100 using ultrasonic dispersion,[48] (as depicted in **Figure 2**A). Initially, the expanded graphite exhibited relatively poor hydrophilicity, with a contact angle of ≈65°. However, after modification with TritonX-100, the super hydrophilic expanded graphite (SHEG) displayed a 0-degree water contact angle, indicating super hydrophilicity. The SHEG maintained its worm-like structure with multiple layers, as shown in Figure 2B and Figure S1 (Supporting Information) and retained its multiple-layer structure after modification (Figure 2C), with no change in appearance (Figure S2, Supporting Information).

The investigation employed LiCl as the sorbent due to its remarkable chemical stability, affordability, and exceptional water sorption capacity. LiCl captured the water molecules that are 5–6 times its weight and shown a capability of removing moisture from an atmosphere even in the very low humidity (up to RH 11.3%) condition. To prepare the LiCl/SHEG composite, the vacuum impregnation technique was used, which eliminated air from the matrix and increased the salt content. The uniform distribution of LiCl crystals on the surface of SHEG was evident in Figure 2D and energy disperse X-ray spectroscopy (EDS) element mapping (Figure 2E; Figure S3, Supporting Information). The uniform distribution of LiCl on the matrix increased the reaction areas, resulting in a faster rate of water vapor sorption. The strong hydrophilicity of SHEG made the matrix more conducive to water vapor sorption and mass transfer.

We compared the moisture sorption performance of LiCl/EG and LiCl/SHEG while maintaining the same mass fraction of salt load. LiCl composite blocks of varying densities were prepared and subjected to water vapor sorption and water leakage tests in the same air atmosphere. The mass change of the pressed LiCl composite in filter paper was monitored over time, and the results were presented in Figure S4 (Supporting Information). Figure 2F explained the water leakage performance after 24 h, which showed that LiCl/SHEG had much better water adhesion ability compared to LiCl/EG. For 400, 500, and 600 kg m^{-3}

© 2024 The Authors. Advanced Energy Materials published by Wiley-VCH GmbH

16146840, 2024, 16, Downloaded from https://onlinelibrary.wiley.com/doi/10.1002/aenm.202303470, Wiley Online Library on [15/07/2024]. See the Terms and Conditions (https://onlinelibrary.wiley.com/terms-and-conditions) on Wiley Online Library for rules of use; OA articles are governed by the applicable Creative Commons License

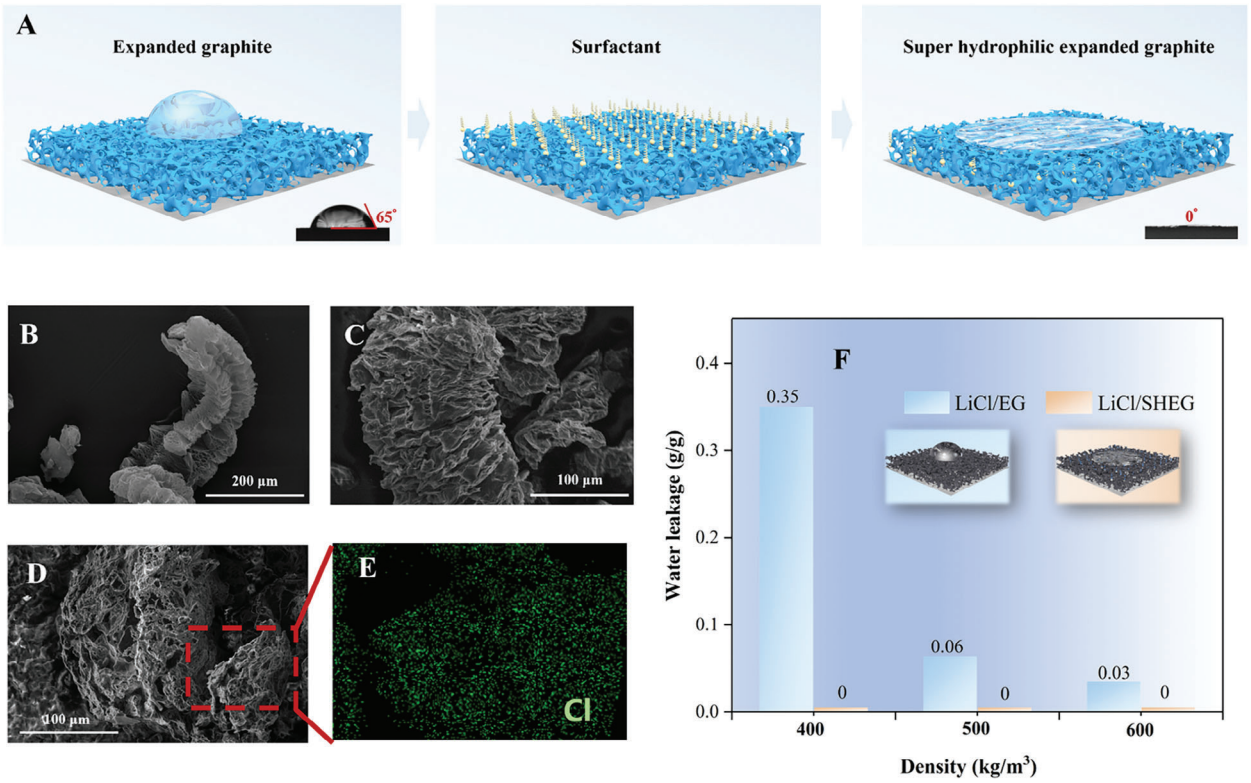

Figure 2. Design, synthesis, and characterization of super hydrophilic expanded graphite. A) The schematic of the synthesis route and the water contact angle of expanded graphite and the super hydrophilic expanded graphite. B) Scanning electron microscopy (SEM) image of expanded graphite. C) Scanning electron microscopy (SEM) image of super hydrophilic expanded graphite, proving the surfactant modification process did not destroy its inner porous structure. D) SEM image of the LiCl/super hydrophilic expanded graphite. E) EDS image of the LiCl/super hydrophilic expanded graphite, proving that LiCl crystals were distributed uniformly in the micropores of the matrix. F) Water leakage performance after 24 h sorption of different densities' LiCl/expanded graphite and LiCl/super hydrophilic expanded graphite blocks.

LiCl/EG blocks, the water leakage in filter paper accounted for 0.35, 0.06, and 0.03 g g^{-1} of the total absorbed water, respectively, while no water leaked out for LiCl/SHEG. The water stains in filters after 48 h of sorption in Figure S4C (Supporting Information) revealed that the leaked-out water of LiCl/EG was significantly more than that of LiCl/SHEG. Additionally, the harvested water of 400, 500, and 600 kg m^{-3} LiCl/SHEG blocks after 24 h was 1.02, 0.89, and 0.79 g g^{-1}, respectively, while the LiCl/EG block uptake was 1.00, 0.84, and 0.72 g g^{-1} moisture for 400, 500, and 600 kg m^{-3} blocks under the same conditions, as shown in Figure S4B (Supporting Information). The study indicated that LiCl/SHEG had greater water sorption and adhesion capacity due to the super hydrophilic ability of the SHEG matrix. The hydrophilic functional groups of hydrophilic materials, such as polyethylene glycol (-OH), provided lone-pair electrons and vacancies that could bond with water vapor molecules through hydrogen bonds or electrostatic interaction.[49,50] Therefore, hydrophilic materials' thermodynamic interaction with water is more favorable than that of hydrophobic materials.

2.3. Water Sorption Performance of LiCl/SHEG

To assess the impact of a porous matrix on sorption performance, the dynamic sorption process of pure LiCl and its composite was measured. **Figure** 3A depicts the sorption kinetics curves of LiCl, LiCl/EG, and LiCl/SHEG at a constant air condition of 25 °C and relative humidity of 60%. The results demonstrate that LiCl/SHEG and LiCl/EG exhibit significantly faster water sorption rates compared to pure LiCl. This is due to the porous matrix providing pores and channels that increase the sorption interface area and support an enhanced mass transfer rate. This is evidenced in Figure 3D, the BET surface area of SHEG was found to be 14 m^2 g^{-1}, which is suitable for particle adsorption. Additionally, the porous structure of SHEG allowed the sorbent to penetrate the voids, porosity, and interlayer space. LiCl/SHEG exhibits a comparable dynamic sorption trend with LiCl/EG in the first hour and subsequently displays a slightly faster sorption rate than LiCl/EG. This is because water's thermodynamic interaction with a super hydrophilic matrix is more favorable than its interactions with an expanded graphite with poor hydrophilicity.

Figure 3B illustrates the moisture uptake performance of LiCl/SHEG at different humidity levels while the temperature remains constant at 25 °C. The results indicate that humidity plays a significant role in the sorption rate, with higher relative humidity levels resulting in higher sorption kinetics. Figure 3C displays the final sorption capacities of the composite, indicating that LiCl/SHEG can harvest 1.06, 1.62, and 3.93 g g^{-1} atmospheric water at RH levels of 40%, 60%, and 80%, respectively. The total absorbed water vapor is much higher in a wet environment with

© 2024 The Authors. Advanced Energy Materials published by Wiley-VCH GmbH

16146840, 2024, 16, Downloaded from https://onlinelibrary.wiley.com/doi/10.1002/aenm.202303470, Wiley Online Library on [15/07/2024]. See the Terms and Conditions (https://onlinelibrary.wiley.com/terms-and-conditions) on Wiley Online Library for rules of use; OA articles are governed by the applicable Creative Commons License

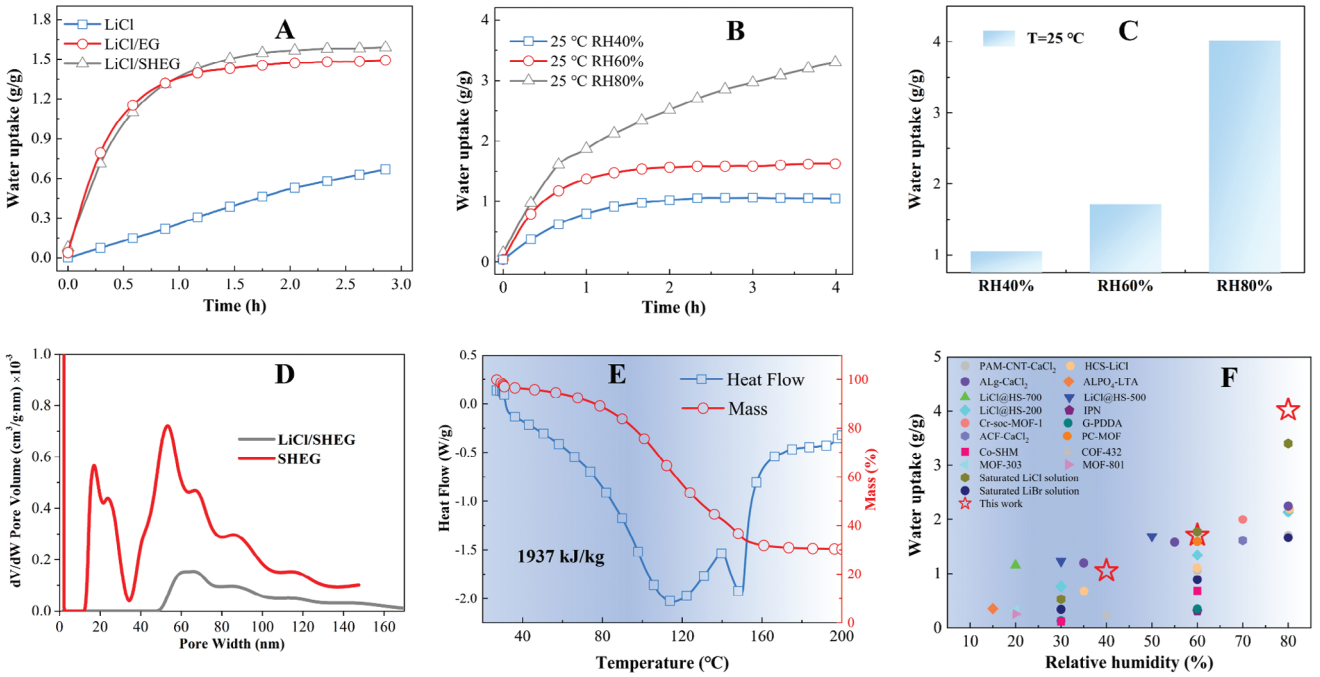

Figure 3. Water sorption and desorption performance of LiCl/super hydrophilic expanded graphite. A) Water uptake performance comparison of LiCl, LiCl/EG, and LiCl/SHEG. B) Water uptake performance of LiCl/SHEG under different humidity with a constant temperature of 25 °C. C) Total water sorption capacity of LiCl/SHEG under different climate conditions. D) Pore size distribution of super hydrophilic expanded graphite matrix and LiCl/super hydrophilic expanded graphite. E) DSC and the thermogravimetric curves of the LiCl/SHEG. F) Total atmosphere water harvesting comparisons of the LiCl/SHEG and previously reported materials.

higher relative humidity levels. Nevertheless, the sorption capacity can reach up to 1.06 g g^{-1} at lower humidity levels (RH 40%). These results indicate that LiCl/SHEG exhibits excellent moisture sorption performance and shows great water harvesting capacity in diverse environments. When compared with reported atmospheric water harvesting materials, LiCl/SHEG displays a higher sorption ability in arid regions (40% RH), semi-humid areas (60% RH), and high humidity (80% RH), as demonstrated in Figure 3F [51–64]

To analyse its desorption performance, differential scanning calorimetry (DSC) and thermogravimetric analysis (TGA) of LiCl/SHEG and LiCl/EG were performed, as shown in Figure 3E and Figure S5 (Supporting Information). The results indicate that the water-releasing process starts ≈30 °C, suggesting that the sorbent can release water under relatively low temperatures suitable for the evaporative cooling system. The total released thermochemical heat of the sorbent accounts for 1937 kJ kg^{-1}, indicating that the sorbent can store a large amount of energy for cooling purposes, demonstrating its superior performance in air cooling.

2.4. Performance of the Membrane Encapsulated LiCl/SHEG

Previous research has often neglected the importance of shape-stabilized performance of sorbents in various application scenarios. This study investigated the moisture sorption performance of a LiCl/SHEG block by pressing the sorbent matrix into a shape-stabilized block that could fit specific application requirements. As shown in Figure S6 (Supporting Information), LiCl/SHEG blocks with a density of less than 400 kg m^{-3} could not maintain a fixed shape. The water absorption and release performance of sorbent blocks at various densities were demonstrated in **Figure** 4A,B, respectively, with an uncompressed LiCl/SHEG composite density of 150 kg m^{-3}. The results showed that uncompressed LiCl/matrix had the highest sorption rate due to its extensive air contact area. However, higher compressed density led to reduced atmospheric water harvesting rate due to decreased heat transfer area. Similarly, the vapor releasing kinetics decreased gradually with improved compressed density. The LiCl/SHEG block with a density of 400 kg m^{-3} was selected for further investigation due to its overall performance, which included being shape-stabilized and maintaining fast kinetics for vapor sorption and desorption.

Deliquescent salts are a type of evaporative cooling material that exhibits superior water harvesting performance, but they can cause agglomeration and solution carryover issues that may be harmful to those who inhale the air. To address these issues, a new method was proposed to confine the LiCl solution inside a PTFE membrane. The porous PTFE membrane is known for its excellent gas permeability, waterproofness, and strong chemical stability, which can solve the problems of salt-solution leakage, cyclic sorption capacity reduction, and metal corrosion issues associated with salts. The LiCl/SHEG sorbent was pressed into a shape-stabilized block and placed on the surface of the PTFE membrane with pore sizes of 3 um closely. The composite sorbent's side was carefully encapsulated with tapes. Figure S7 (Supporting Information) confirmed the breathable and waterproof ability of PTFE, with a water contact angle of ≈120°, indicating its

© 2024 The Authors. Advanced Energy Materials published by Wiley-VCH GmbH

16146840, 2024, 16, Downloaded from https://onlinelibrary.wiley.com/doi/10.1002/aenm.202303470, Wiley Online Library on [15/07/2024]. See the Terms and Conditions (https://onlinelibrary.wiley.com/terms-and-conditions) on Wiley Online Library for rules of use; OA articles are governed by the applicable Creative Commons License

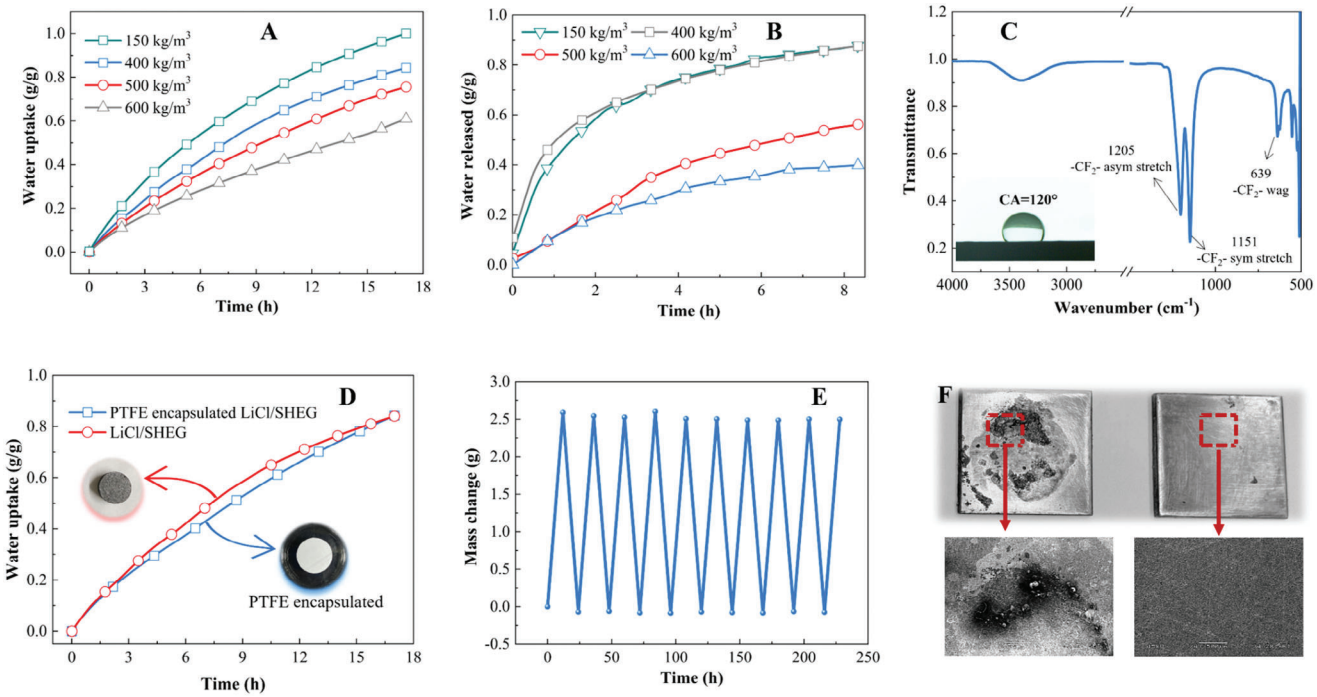

Figure 4. Performance of PTFE membrane encapsulated LiCl/super hydrophilic expanded graphite. A) Water uptake performance comparison of LiCl/SHEG blocks under the climate 25 °C and RH60%. B) Water releasing performance of LiCl/SHEG blocks under 55 °C. C) The FTIR spectrum and water contact angle of the PTFE membrane. D) Water uptake performance comparison of LiCl/SHEG and PTFE encapsulated blocks under the climate 25 °C and RH60%. E) The cycling performance of the PTFE encapsulated LiCl/SHEG blocks; F) Corrosion assessment. Photos and SEM images of stainless-steel plate after seven absorption and desorption cycles. Left, the plate directly in contact with salt sorbent; right, the plate directly in contact with PTFE membrane encapsulated salt sorbent.

outstanding hydrophobicity (Figure 4C). Moreover, the two characteristic peaks of PTFE target spectrum indicated its strong C—C bonds and C—F bonds, which also contributed to its hydrophobicity. Figure 4D compared the moisture sorption performance of LiCl/SHEG and the membrane-encapsulated LiCl/SHEG. The LiCl/SHEG had similar dynamic sorption trends with the PTFE encapsulated ones, indicating the excellent air permeability of the porous PTFE. Furthermore, the membrane-wrapped sorbent had superior waterproof performance. After seven days of atmospheric water harvesting, the LiCl solution was well confined inside the membrane, with no signs of salt solution leakage (Figure S8, Supporting Information). The water sorption capacity of the PTFE encapsulated LiCl/SHEG under different climate conditions can be found in Figure S9 (Supporting Information). The proposed PTFE encapsulated LiCl/SHEG composite combines the dual advantages of fast sorption kinetics of salt-based composite sorbents and superior water adhesion ability without any risk of solution leakage, thanks to the excellent permeability and waterproofness of the membrane.

The use of sorbents in cooling systems can be hindered by the corrosive effects of salt solutions on metal components. However, a new approach has been developed to fully address this issue. To test the effectiveness of this approach, a corrosion test was conducted between the LiCl matrix and the encapsulated sorbent. The sorbent was in direct contact with stainless-steel plates during seven absorption and desorption tests. The results, depicted in Figure 4F and Figure S10 (Supporting Information), revealed that the stainless-steel plate in contact with the non-encapsulated sorbent was severely corroded due to the presence of halide ions on metals. Conversely, the plate in contact with sorbents encapsulated in membranes remained smooth after cycling, with no corrosion observed in the SEM figure. This indicates that the liquid containing halide ions did not leak through the PTFE membrane. Moreover, the cycling performance of the proposed membrane-wrapped LiCl/SHEG composite was tested over ten absorption-desorption cycles, with Figure 4E showing no significant degradation in sorption performance. This indicates excellent stability and reusability, which combined with the superior water sorption for a wide range of relative humidity, exceptional chemical stability, and corrosion prevention offered by the PTFE encapsulated LiCl/SHEG, provides significant potential for direct evaporative cooling, leading to cost and maintenance reductions.

2.5. The Cooling Performance of the Sorbent Cooler

To test the temperature change of the sorbent room and reference room under different climate conditions, both were placed inside a constant temperature and humidity chamber (QHP-150BE, LICHEN Technology, ±0.1 °C; ±2% RH). Two fans with a power of 0.8 W were installed at the inlet boundary, and the flow velocity was measured by the TESTO 400. Nine temperature sensors were distributed at the top, middle, and bottom of the rooms, and the temperature data were collected using an Agilent data collector (34970A, Agilent), from which the average room temperature was calculated. The reference room was placed above an

© 2024 The Authors. Advanced Energy Materials published by Wiley-VCH GmbH

16146840, 2024, 16, Downloaded from https://onlinelibrary.wiley.com/doi/10.1002/aenm.202303470, Wiley Online Library on [15/07/2024]. See the Terms and Conditions (https://onlinelibrary.wiley.com/terms-and-conditions) on Wiley Online Library for rules of use; OA articles are governed by the applicable Creative Commons License

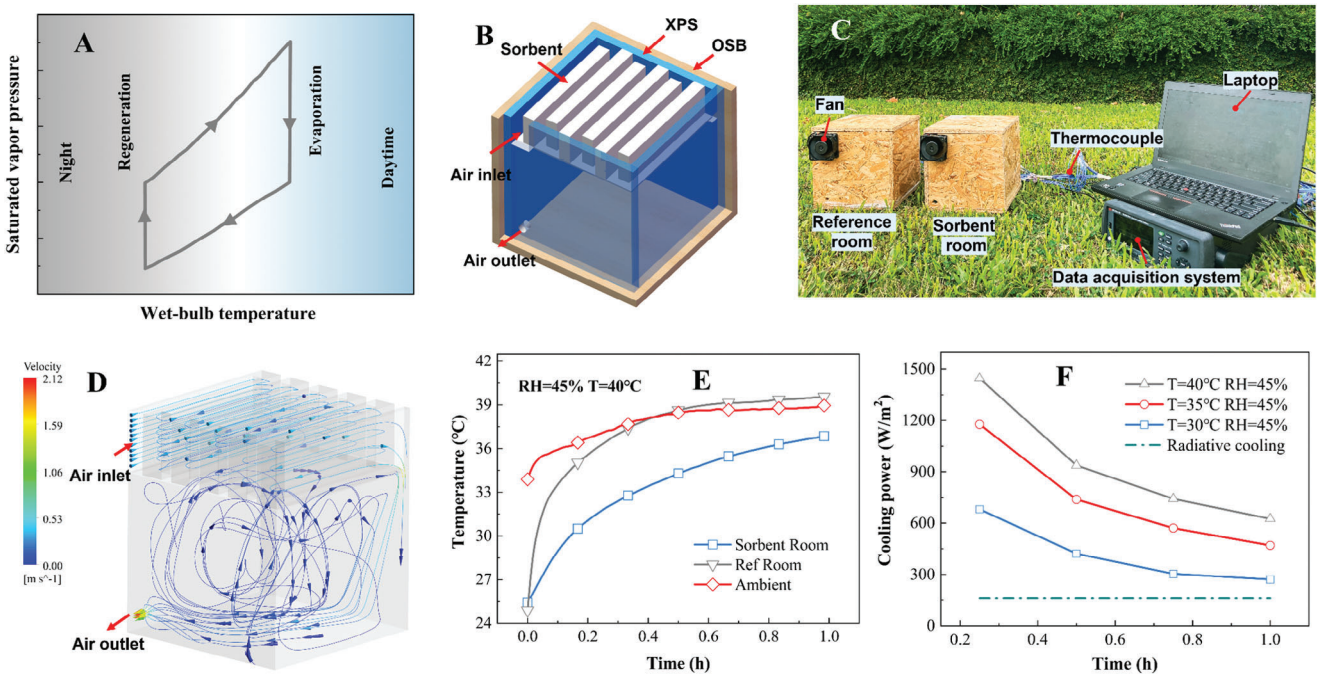

Figure 5. Experimental results of the PTFE membrane encapsulated LiCl/SHEG sorbent evaporative cooling room. A) The schematic of the working cycle of the vapor sorption and desorption of the PTFE membrane encapsulated LiCl/SHEG sorbent. B) Schematic diagram of the experimental room of the sorbent room. C) Photograph of the reference room and sorbent room system. D) The velocity and streamline distribution of the flowing air. E) Temperature compares between the sorbent room and reference room when the climate is 40 °C, RH45%. F) Cooling power profile of sorbent room under different climate conditions and the comparison with radiative cooling.

electronic balance (SAN JIANG, range 5000 g, 0.01 g) to record its weight loss over time. Both the sorbent room and reference room were placed inside the chamber with a climate of 25 °C and relative humidity of 60% for 12 h to achieve the atmospheric water harvesting process. Then, they were moved to the test climate chamber to measure the evaporative cooling performance, and the temperatures of the two rooms and the sorbent mass change were recorded. The resulting cooling power is calculated as shown in Equation (1).

Figure 5A illustrates the operational concept of the sorbent evaporative cooling system. To examine the efficacy of the cooling sorbent concept, an experimental room was constructed and outfitted with the sorbent cooling system. The building model consisted of oriented strand board (OSB) and extruded polystyrene boards (XPS) each with a thickness of 10 mm, as illustrated in Figure 5B and Figure S11 (Supporting Information). Positioned directly above the room was a sorbent channel that held a rectangular block of super hydrophilic expanded graphite/LiCl sorbent with a density of 400 kg m^{-3}. The sorbent was pressed to maintain a high mass transfer rate and shape stabilization. Ten plates of shape-stabilized PTFE membrane-encapsulated LiCl/SHEG sorbent were integrated into the ventilation channel. Our PTFE membrane encapsulated LiCl/SHEG material showed excellent water adhesion, waterproofing, and shape-stabilization properties, enabling direct integration of the sorbent matrix into the building ventilation channel while avoiding water leakage and solution carryover.

The experimental system was designed to test the system's application in diverse climatic regions, and a reference room without the evaporative cooling component was also set up to compare the cooling performance of the evaporative cooling rooms, as shown in Figure 5C. A small fan, with a working power of 0.8 W, was installed at the channel inlet to provide consistent airflow, and the airflow rate was maintained at 0.3–0.4 m s^{-1}. The airflow distribution was simulated using Fluent software, as illustrated in Figure 5D. The airflow moved through the sorbent channel and circulated evenly in the indoor room before flowing out to complete the cooling process. To evaluate the indoor evaporative cooling performance of the processed experimental room model, it was placed in a constant temperature and humidity chamber. The experimental and reference rooms were subjected to different conditions, including three temperature settings (30, 35, and 40 °C) while the relative humidity was maintained at 45%.

Figure 5E and Figure S12 (Supporting Information) depict the temperature curves of the sorbent room and reference room at different temperature conditions. As the exterior environment temperature increases to 40 °C, the temperatures of both rooms increase gradually from the initial air temperature of 25 °C to the chamber temperature. However, the sorbent room exhibits a significantly lower temperature than the reference room. The evaporative ventilation system shows superior performance in higher temperature climates, with temperature drops of 0.6, 1.8, and 3.5 °C after 1 h of operation when the ambient temperature is 30 °C, 35 °C, and 40 °C, respectively. This temperature drop occurs due to the heat absorption of the sorbent, which absorbs the heat of the flowing air and reduces its temperature. The desorption process is more efficient in higher temperature climates, thanks to improved kinetics, and the high thermal conductivity

© 2024 The Authors. Advanced Energy Materials published by Wiley-VCH GmbH

16146840, 2024, 16, Downloaded from https://onlinelibrary.wiley.com/doi/10.1002/aenm.202303470, Wiley Online Library on [15/07/2024]. See the Terms and Conditions (https://onlinelibrary.wiley.com/terms-and-conditions) on Wiley Online Library for rules of use; OA articles are governed by the applicable Creative Commons License

of the expanded graphite matrix accelerates the heat transfer between the air and the sorbent, resulting in rapid air cooling.

Additional experimental tests were conducted to explore the cooling performance under varying humidity conditions while maintaining a constant temperature of 30 °C. As demonstrated in Figure S13 (Supporting Information), it becomes evident that humidity also plays a crucial role in affecting the cooling performance. When the humidity is lower (RH 45%), the sorbent room experiences a temperature drop of 0.6 °C compared to the reference room after 1 h of cooling. As the humidity level rises to 60%, the temperature in the sorbent room is 0.48 °C lower than in the reference room. It is worth noting that under relatively higher humidity conditions (RH 75%), after 1 h of operation, the temperature in the sorbent room exceeds that of the reference room. This discrepancy arises from the fact that when humidity is high, the sorbent material remains in the absorption process. During the water harvesting phase, it releases heat, resulting in a slightly higher temperature in the sorbent room compared to the reference room. This observation suggests that this cooling method may not be suitable for regions with high humidity levels.

The weight loss profile of the sorbent cooler room (Figure S14, Supporting Information) indicates the amount of water evaporated during the test. The averaged cooling power was calculated using Equation (1), where H is the enthalpy of vaporization of water (2450 J g^{-1}) and S is the surface area of the indoor room (0.0256 m^{-2}) in this work. The cooling power of the sorbent during the test is shown in Figure 5F. A high cooling power value is observed at the beginning of the test due to the large temperature difference between the ambient air and the sorbent room. As the test progresses, the cooling power gradually decreases but still exhibits a high cooling capacity even after one hour of operation. The cooling power reaches up to 630, 470, and 272 W m^{-2} for climates of 40, 35, and 30 °C, respectively, which is significantly higher than the radiative cooling power (depicted in Figure 1D) and 4 times higher than the theoretically highest power of radiative cooling (160 W m^{-2}). The cooling power of the sorbent is higher with an increase in the outdoor temperature, which is consistent with previous results. These results demonstrate that the sorbent cooler can provide adequate evaporative cooling capacity to an indoor room without any extra water consumption, thereby satisfying the space cooling demand and bringing better energy conversion performance.

2.6. Energy Saving and CO_2 Mitigation Potential Assessment

This work introduced a novel solution to combat the rising frequency and intensity of heat waves worldwide, specifically with a question of understanding how well this cooling technology performs under varying climatic conditions if integrated into a real-time building as per the ASHRAE standards, both from energy savings and carbon dioxide mitigation potential point of view. A one-story small office building that closely resembles an actual office facility was modelled in EnergyPlus (refer Figure S15 and Tables S2 and S3, Supporting Information for schematic view and construction material layers) and leveraged in nine cities, including Hong Kong, Shanghai, Mumbai, Abu Dhabi, Sydney, New York, Paris, Sao Paulo, and Cape Town that experience different climates and has a distinct electricity emission (as depicted in Table S8, Supporting Information) based on the energy mix.

Figure 6B,C depict the results of cooling energy usage and energy savings for the reference building and the building with sorbent cooler modelled in EnergyPlus, the carbon footprint of cooling energy used in reference building and the building with sorbent cooler modelled in SimaPro, and carbon dioxide mitigation potential by shifting to sorbent cooling. The cooling energy use and energy savings annual summary in nine different cities; monthly summary of cooling energy use and energy savings for each city can be seen in Figures S16–S24 (Supporting Information). Our preliminary results with small-scale building models showed that our proposed sorbent cooler can reduce annual cooling energy use by of 12.16% to 39% compared with predictions for nine cities with different climates. The highest reduction percentage was observed in Abu Dhabi, while Paris showed the lowest reduction percentage. The difference in percentage is mainly attributed to the varied energy consumption by cooling and fans in different months due to localized weather conditions in different cities. For example, Hong Kong's monthly cooling energy for sorbent roofs ranged from 19.8 to 2285.8 kWh throughout the year, while it ranged from 224.23 to 3230 kWh for reference buildings (Figure S16, Supporting Information). The annual energy savings varied across the cities, with Hong Kong, Shanghai, Mumbai, Abu Dhabi, Sydney, New York, Paris, Sao Paulo, and Cape Town showing savings of 6269.53, 3790.99, 9701.39, 3848.62, 3848.62, 2470.88, 1205.03, 4879.29, and 3478.54 kWh, respectively.

According to Figure 6D,E, the carbon footprint of cooling energy use in buildings equipped with camel fur-inspired sorbent cooling technology is lower than in reference buildings. The potential annual carbon footprint saving with our sorbent cooler per city ranges from 0.09 to 13.62 tCO_2-eq., which is ≈61% to 87.83% decrease when compared to emissions released from cooling energy usage in reference building. The carbon mitigation potential varied across the cities, with 5.48 tCO_2-eq. for Hong Kong, 3.24 tCO_2-eq. for Shanghai, 13.62 tCO_2-eq. for Mumbai, 2.70 tCO_2-eq. for Abu Dhabi, 3.73 tCO_2-eq. for Sydney, 0.57 tCO_2-eq. for New York, 0.09 tCO_2-eq. for Paris, 0.69 tCO_2-eq. for Sao Paulo, and 3.73 tCO_2-eq. for Cape Town, respectively. This indicates that the energy consumed by the buildings equipped with sorbent cooling technology emitted lower levels of CO_2 than the reference buildings.

The effectiveness of camel fur-inspired sorbent coolers in buildings across different cities was demonstrated, and extensive building energy simulations conducted worldwide to see the potential of this novel solution to combat the rising frequency and intensity of heat waves worldwide (**Figure 6A**),[65] specifically with a question of understanding how well this cooling technology performs under varying climatic conditions if integrated into a real-time building. The global simulations revealed the practical applicability of this technology for annual cooling energy savings, as shown in Figure 6F. The results indicate that sorbent coolers are most effective in climates such as tropical savannas, humid subtropical and tropical and sub-tropical deserts, followed by Mediterranean and western Europe oceanic climates. These findings reveal the energy performance of sorbent coolers and suggest their potential use in specific cities. This information can

© 2024 The Authors. Advanced Energy Materials published by Wiley-VCH GmbH

16146840, 2024, 16, Downloaded from https://onlinelibrary.wiley.com/doi/10.1002/aenm.202303470, Wiley Online Library on [15/07/2024]. See the Terms and Conditions (https://onlinelibrary.wiley.com/terms-and-conditions) on Wiley Online Library for rules of use; OA articles are governed by the applicable Creative Commons License

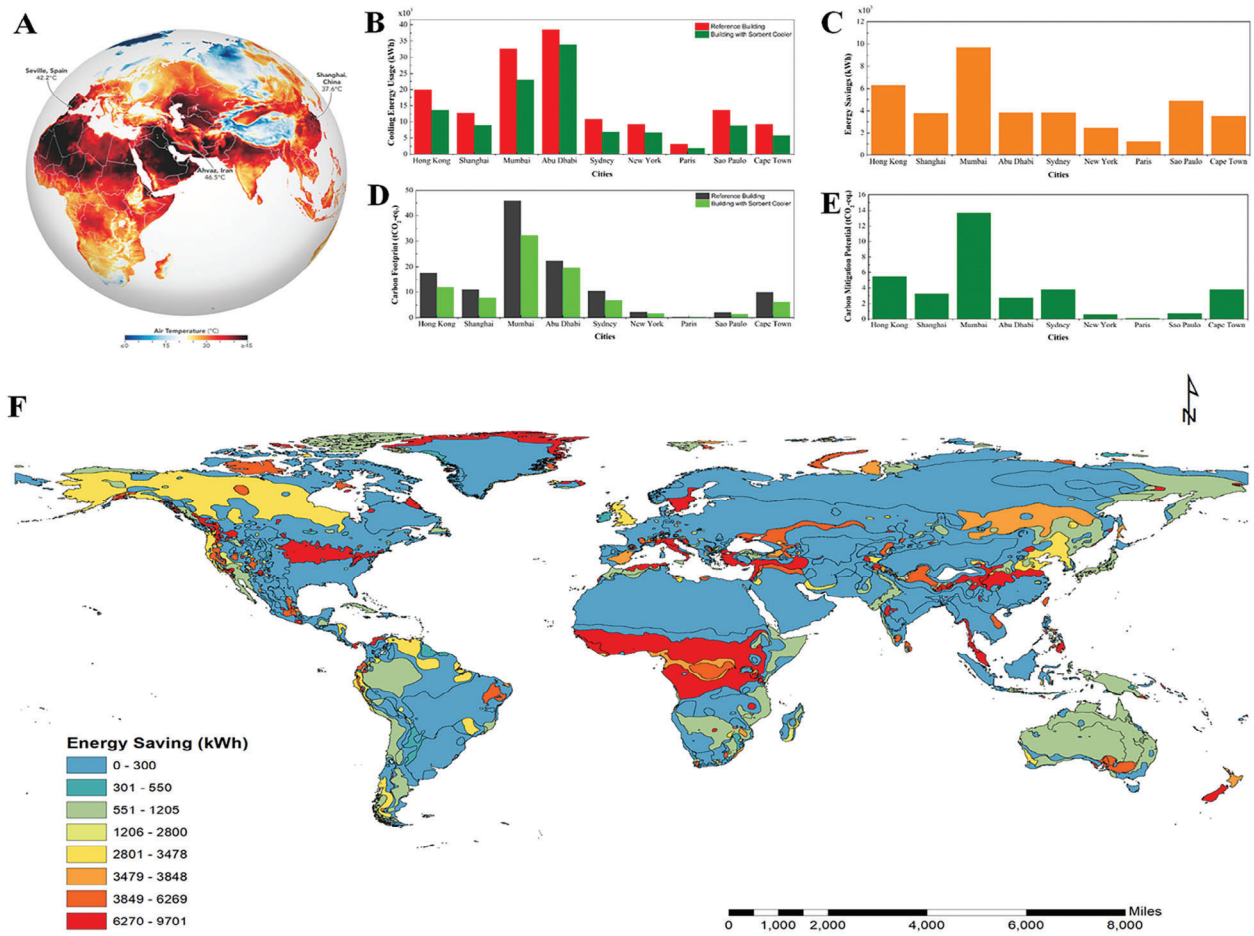

Figure 6. A) Global heat waves in June and July 2022.[65] B) Cooling energy usage (kWh) for the reference building and the building with sorbent cooler. C) Energy savings for the reference building and the building with sorbent cooler. D) Carbon footprint of cooling energy used in reference building and the building with sorbent cooler. E) Carbon dioxide mitigation potential in nine selected cities by using our sorbet cooler. F) Simulated world map showing the sorbent cooling technology potential in annual cooling energy saving in different climate zones. (Note: energy usage was modelled in EnergyPlus and carbon footprint was simulated in SimaPro). Nine representative cities (Hong Kong, Shanghai, Mumbai, Abu Dhabi, Sydney, New York, Paris, Sao Paulo, Cape Town) from different zones were selected for comparison. This theoretical model implies that the proposed sorbent cooler can reduce annual cooling energy use by of 12.16% to 39% compared with predictions for nine cities with different climates and has the potential to cut down cooling energy carbon emission by 61% to 87.83% when compared to emissions released from cooling energy usage in reference building.

help drive the net energy zero mission in buildings and promote global cooling and sustainability.

3. Conclusion

This study has resulted in the successful development of a passive cooling sorbent capable of absorbing water vapor from the atmosphere for cooling purposes in the buildings. The sorbent is designed with an innovative breathable membrane that encapsulates a super hydrophilic matrix. We proposed a hydrophilic modified expanded graphite to improve water adhesion to salt, resulting in the LiCl/SHEG design capable of harvesting up to 3.93 g g^{-1} atmospheric water. This sorbent demonstrates exceptional performance in arid, semi-humidity, and high humidity regions. Additionally, the encapsulated membrane is both breathable and waterproof, allowing for airflow while preventing water leaks. This novel material is shape-stabilized, has excellent cycling performance, and remarkable water adhesion ability. It also overcomes the swelling issue of salt, prevents carryover of liquid sorbent, and avoids salt's corrosive performance.

The sorbent cooler's cooling ability was demonstrated in sorbent room model experiments, showing that the sorbent room's temperature could be lowered by up to 5 °C compared to the reference room. The resulting cooling power was 630 W m^2 (RH@45%, T@40 °C), which is four times higher than the theoretically highest power of radiative cooling. With a predicted 20% increase in building area this decade, adding a total surface area of nearly 45 billion m^2, it is crucial to consider the 1.2 billion people in poor rural areas who lack access to cooling. By adopting this approach, more cooling capacity can be generated for these areas, reducing CO_2 emissions and saving cooling energy. Our theoretical model suggests that the proposed sorbent cooler can reduce annual cooling energy use by of 12.16% to 39% compared with predictions for nine cities with different climates and has the

© 2024 The Authors. Advanced Energy Materials published by Wiley-VCH GmbH

16146840, 2024, 16, Downloaded from https://onlinelibrary.wiley.com/doi/10.1002/aenm.202303470, Wiley Online Library on [15/07/2024]. See the Terms and Conditions (https://onlinelibrary.wiley.com/terms-and-conditions) on Wiley Online Library for rules of use; OA articles are governed by the applicable Creative Commons License

potential to cut down cooling energy carbon emission by 61% to 87.83% when compared to emissions released from cooling energy usage in reference building. This investigation presents an eco-friendly, energy-efficient, and low technical barriers cooling strategy, providing a new pathway for efficient daytime evaporative cooling without additional water supply. Overall, our findings have significant implications for various building energy, and air-cooling applications.

While our cooling method presents several advantages, such as being passive, environmentally friendly, and easily accessible, it is essential to acknowledge certain limitations. One significant limitation is its suitability in high-humidity regions, as discussed previously. Additionally, we recognize that further research and refinement may be required to optimize its performance in specific conditions or applications. We are committed to exploring these limitations and potential areas for improvement in future studies.

4. Experimental Section

Material Preparation: 99.995% pure lithium chloride, Triton-100, 80-mesh expanded graphite, and porous PTFE membranes were procured. Macklin was the supplier of Lithium chloride (99.995%) and Triton-100 while the 80-mesh expanded graphite was provided by Tengshengda, China. Porous PTFE membranes were supplied by the New Polyfluorine material company, China.

To prepare super hydrophilic expanded graphite, the expanded graphite was first dried in a vacuum oven for 12 h at 100 °C to eliminate water. TritonX-100 was dissolved in ethanol and mixed well in a mass fraction of surfactant to expanded graphite of 1:10. The dry expanded graphite was added to the ethanol solution and dispersed ultrasonically for 20 min, repeated three times, and left to stand for 12 h. The material was then collected by vacuum filtration and dried at 80 °C for 12 h to remove ethanol, resulting in super hydrophilic EG.

To prepare LiCl/super hydrophilic expanded graphite, the hydrophilic expanded graphite was dried at 100 °C for 12 h, then immersed in a 30 wt.% LiCl solution and placed inside a vacuum chamber for 8 h. Next, the LiCl/matrix was filtered to remove the extra salt solution. The collected material was then dried at 120 °C for 8 h in a vacuum heating chamber to obtain the LiCl/super hydrophilic expanded graphite composite.

To create a PTFE membrane encapsulated sorbent, the prepared LiCl/matrix composite was pressed into a shape-stabilized block with a specific density. The block was then placed on the surface of a PTFE membrane with a 3 µm pore size and encapsulated carefully with high-temperature tapes.

Material Characterization: An FEI Quanta 450 FEG SEM to capture SEM images and EDX mapping images was used. The specific surface area (BET) and pore volume were determined at 77 K using a Micromeritics ASAP 2020 apparatus and porosity analyzer. Contact angles were measured via the sessile drop method with a 10 µL water droplet as the indicator and recorded with a digital camera (Basler, ace acA1300-200um). To measure the DSC and TG, we employed a Perkin Elmer Diamond DSC and kept the nitrogen flow rate constant at 50 mL min^{-1}. The infrared spectra were measured using a Fourier transform infrared spectrometer (Bruker Tensor 27 FTIR Spectrometer). Water sorption under constant RH was evaluated and different temperatures using the constant temperature and humidity testing machine (QHP-150BE, LICHEN Technology, ±0.1 °C; ±2% RH) while recording the mass change of the sample using an electronic balance (YOUSHENG, 0.1 mg).

Stability Test: Ten cycles of sorption-desorption were conducted to assess the cycling performance of the PTFE encapsulated LiCl/SHEG, using a shape-stabilized 400 kg m^{-3} block placed iF. The mass before and after each absorption/desorption cycle was measured using an electronic balance (YOUSHENG, 0.1 mg).

Corrosion test: To test the corrosivity of the PTFE encapsulated and non-encapsulated 400 kg m^{-3} LiCl/SHEG block, pure stainless-steel plates measuring 2 cm × 2 cm were placed in direct contact with the sorbents. The plates were exposed to ambient conditions of 22 to 24 °C and 63% to 75% relative humidity for 23 h, followed by heating on a hot plate at 120 °C for 1 h to simulate working cycling.

Fabrication of Sorbent Room Model: The sorbent room and the reference room were constructed using oriented strand board (OSB, thickness: 10 mm) and extruded polystyrene boards (XPS, thickness: 10 mm). OSBs are commonly used in building construction for wall sheathing, floor underlayment, and roof covers in both residential and commercial buildings. The XPS was a laminated insulating board that was safe, environmentally friendly, healthy, non-toxic, and moisture-proof. The experimental rooms' total dimensions were 200×200×200 mm, and the sorbent channel, which measures 160×160×50 mm, was made of acrylic board with a thickness of 2 mm. The bottom and top of the channel were designed with 1 mm thick grooves to secure the shape-stabilized sorbent. It was integrated ten plates of encapsulated sorbents, measuring 138×48×8 mm, into the ventilation channel. A total of 212 g LiCl/SHEG was used, and the channel was placed directly above the room (Figure S11, Supporting Information).

Energy Saving Assessment: Building energy simulations in EnergyPlus are carried out to assess the energy performance and determine how this cooling technology would perform in varying climatic conditions. To achieve this, we selected a one-story small office building that closely resembled real office facilities and used it as the basis for modelling a reference building and a building with a sorbent-based roof (see Figure S15, Supporting Information). The ASHRAE code of the building was SmallOffice-ASHRAE 169-2013-2A. We have provided the details of the materials used for wall and roof construction in both buildings and their respective properties in Note 2 in Supporting Information and Tables S2–S7 (Supporting Information).

Once the building designs were finalized, it was performed building energy simulations on both buildings to estimate the variation in cooling energy use and energy-saving potential. First, nine different cities with suitable weather files in .epw formats downloaded from EnergyPlus was selected. Then, it was conducted extensive simulations to understand the energy-saving potential of a sorbent-based cool roof on a global scale. ArcGIS to visualize the energy-saving potential worldwide was utilized. To achieve this, a shapefile of the world map with climate zones attributed to shape area and shape length as a layer was added. It was also created a separate layer on energy-saving potential based on the building energy simulations outputs, attributing to climate zones as in the shape file. Using the analysis command protocols in ArcGIS, the building energy simulations file futures to the shapefile for visualization was joined.

Carbon Mitigation Potential Assessment: The environmental performance of a camel fur-based sorbent cool roof in comparison with a reference building under the building energy efficiency improvement standards is estimated by evaluating the carbon mitigation potential, see Eq. (2).

$$\mathrm{CMP} = \mathrm{GHG}_{\mathrm{en\_ref\_roof_c}} - \mathrm{GHG}_{\mathrm{en\_sorbent\_cool\_roof_c}} \quad (2)$$

where $GHG_{en\_ref\_roof_c}$ is the greenhouse gas (GHG) emission due to cooling energy use in reference building in cities c that experience varying climatic conditions in tCO_2-eq.; $GHG_{en\_sorbent\_cool\_roof_c}$ is the GHG emission due to cooling energy use in sorbent cool roof building in cities c that experience varying climatic conditions in tCO_2-eq.

The GHG emission released due to cooling energy use in both reference and sorbent-based cool roof buildings are modelled by considering scope 2 (emissions that occurred out of the office building maintenance team control but as a result of electricity the office directly consumed from the grid) and scope 3 (emissions in the electricity supply chain of the grid) electricity emissions from the Ecoinvent database. Also, accounting for the practical situation that most office buildings are connected to the national electric grid in respective cities, the emissions released due to transmission and distribution (T&D) losses are considered. Eq. (3) represents the GHG emissions model used in this study to estimate the total GHG

© 2024 The Authors. Advanced Energy Materials published by Wiley-VCH GmbH

16146840, 2024, 16, Downloaded from https://onlinelibrary.wiley.com/doi/10.1002/aenm.202303470, Wiley Online Library on [15/07/2024]. See the Terms and Conditions (https://onlinelibrary.wiley.com/terms-and-conditions) on Wiley Online Library for rules of use; OA articles are governed by the applicable Creative Commons License

emissions. The electricity emission factors data of the nine selected cities can be seen in Table S8 (Supporting Information).

$$GHG_{en\_building\_c} = EleC_{building,c} \times \left(Scope\ 2_{ele,c,g} + Scope\ 3_{ele,c,g} + T\&D\ Losses_{ele,c,g}\right) \quad (3)$$

where $GHG_{en\_building\_c}$ is the GHG emission due to electrical energy consumption (*EleC*) in the building located in city *c*; *ele* is the electricity mix accounting for both traditional and new forms of energy; *g* is the grid to which the building is connected in a given climate given multiple grid networks are available.

Supporting Information

Supporting Information is available from the Wiley Online Library or from the author.

Conflict of Interest

The authors declare no conflict of interest.

Author Contributions

W.L. and X.Y. contributed equally to this work.

Data Availability Statement

The data that support the findings of this study are available from the corresponding author upon reasonable request.

Keywords

evaporative-cooling, hygroscopic membrane, sorbent cooler, space cooling, ultrahigh cooling power

Received: October 15, 2023
Revised: December 19, 2023
Published online: February 26, 2024

[1] Annual 2022 Global Climate Report. National Centres for Environmental Information">Annual 2022 Global Climate Report. National Centres for Environmental Information.
[2] R. Khosla, N. D. Miranda, P. A. Trotter, A. Mazzone, R. Renaldi, C. McElroy, F. Cohen, A. Jani, R. Perera-Salazar, M. McCulloch, *Nat. Sustain.* **2021**, *4*, 201.
[3] L. Yang, H. Yan, J. C. Lam, *Appl. Energy* **2014**, *115*, 164.
[4] S. Perkins-Kirkpatrick, S. Lewis, *Nat. Commun.* **2020**, *11*, 3357.
[5] S. G. Yalew, M. T. H. van Vliet, D. E. H. J. Gernaat, F. Ludwig, A. Miara, C. Park, E. Byers, E. De Cian, F. Piontek, G. Iyer, I. Mouratiadou, J. Glynn, M. Hejazi, O. Dessens, P. Rochedo, R. Pietzcker, R. Schaeffer, S. Fujimori, S. Dasgupta, S. Mima, S. R. S. da Silva, V. Chaturvedi, R. Vautard, D. P. van Vuuren, *Nat. Energy* **2020**, *5*, 794.
[6] K. Ellsworth-Krebs, *Nat. Energy* **2020**, *5*, 20.
[7] L. T. Biardeau, L. W. Davis, P. Gertler, C. Wolfram, *Nat. Sustain.* **2020**, *3*, 25.
[8] B. K. Bose, *IEEE Transactions on Industrial Electronics* **2012**, *60*, 2638.
[9] E. Derkenbaeva, S. H. Vega, G. J. Hofstede, E. Van Leeuwen, *Renew. Sustain. Energy Rev.* **2022**, *153*, 111782.
[10] M. M. Hossain, M. Gu, *Adv. Sci.* **2016**, *3*, 1500360.
[11] T. Li, Y. Zhai, S. He, W. Gan, Z. Wei, M. Heidarinejad, D. Dalgo, R. Mi, X. Zhao, J. Song, J. Dai, C. Chen, A. Aili, A. Vellore, A. Martini, R. Yang, J. Srebric, X. Yin, L. Hu, *Science* **2019**, *364*, 760.
[12] X. Sun, Y. Sun, Z. Zhou, M. A. Alam, P. Bermel, *Nanophotonics* **2017**, *6*, 997.
[13] C. Feng, P. Yang, H. Liu, M. Mao, Y. Liu, T. Xue, *Nano Energy* **2021**, 85.
[14] J. Mandal, Y. Yang, N. Yu, A. P. Raman, *Joule* **2020**, *4*, 1350.
[15] D. Zhao, A. Aili, Y. Zhai, J. Lu, D. Kidd, G. Tan, X. Yin, R. Yang, *Joule* **2019**, *3*, 111.
[16] B. Fumey, R. Weber, L. Baldini, *Renew. Sustain. Energy Rev.* **2019**, *111*, 57.
[17] D. Lefebvre, F. H. Tezel, *Renew. Sustain. Energy Rev.* **2017**, *67*, 116.
[18] A. Gil, M. Medrano, I. Martorell, A. Lázaro, P. Dolado, B. Zalba, L. F. Cabeza, *Renew. Sustain. Energy Rev.* **2010**, *14*, 31.
[19] Y. Yang, G. Cui, C. Q. Lan, *Renew. Sustain. Energy Rev.* **2019**, *113*, 109230.
[20] M. Alberghini, S. Hong, L. M. Lozano, V. Korolovych, Y.i Huang, F. Signorato, S. H. Zandavi, C. Fucetola, I. Uluturk, M. Y. Tolstorukov, G. Chen, P. Asinari, R. M. Osgood, M. Fasano, S. V. Boriskina, *Nat. Sustain.* **2021**, *4*, 715.
[21] Y. Tu, R. Wang, Y. Zhang, J. Wang, *Joule* **2018**, *2*, 1452.
[22] M. M. Rafique, P. Gandhidasan, H. M. Bahaidarah, *Renew. Sustain. Energy Rev.* **2016**, *56*, 179.
[23] X. Chen, S. Riffat, H. Bai, X. Zheng, D. Reay, *Energy and Built Environment* **2020**, *1*, 106.
[24] H. Shan, Q. Pan, C. Xiang, P. Poredos, Q. Ma, Z. Ye, G. Hou, R. Wang, *Cell Reports Physical Science* **2021**, 00664.
[25] E. Krüger, E. González Cruz, B. Givoni, *Build. Environ.* **2010**, *45*, 1422.
[26] A. Sharifi, Y. Yamagata, *Appl. Energy* **2015**, *160*, 336.
[27] C. Wang, L. Hua, H. Yan, B. Li, Y. Tu, R. Wang, *Joule* **2020**, *4*, 435.
[28] R. Li, Y. Shi, L. Shi, M. Alsaedi, P. Wang, *Environ. Sci. Technol.* **2018**, *52*, 5398.
[29] Y. Zhang, R. Wang, T. Li, *Energy* **2018**, *156*, 240.
[30] F. B. Cortés, F. Chejne, F. Carrasco-Marín, A. F. Pérez-Cadenas, C. Moreno-Castilla, *Energy Convers. Manage* **2012**, *53*, 219.
[31] B. Wang, X. Zhou, Z. Guo, W. Liu, *Nano Today* **2021**, *40*, 101283.
[32] T. Li, R. Wang, J. Kiplagat, L. Wang, *Appl. Energy* **2009**, *86*, 1201.
[33] K. Korhammer, M.-M. Druske, A. Fopah-Lele, H. U. Rammelberg, N. Wegscheider, O. Opel, T. Osterland, W. Ruck, *Appl. Energy* **2016**, *162*, 1462.
[34] Y. Fang, W. Diao, J. Su, X. Liang, S. Wang, X. Gao, Z. Zhang, *Sol. Energy Mater. Sol. Cells* **2021**, *230*, 111221.
[35] Y. Zhang, R. Wang, *Energy Storage Mater.* **2020**, *27*, 352.
[36] S. Xi, L. Wang, H. Xie, W. Yu, *ACS Nano* **2022**, *16*, 3843.
[37] T. Li, Y. Zhai, S. He, W. Gan, Z. Wei, M. Heidarinejad, D. Dalgo, R. Mi, X. Zhao, J. Song, J. Dai, C. Chen, A. Aili, A. Vellore, A. Martini, R. Yang, J. Srebric, X. Yin, L. Hu, *Science* **2019**, *364*, 760.
[38] A. P. Raman, M. A. Anoma, L. Zhu, E. Rephaeli, S. Fan, *Nature* **2014**, *515*, 540.
[39] J. Song, W. Zhang, Z. Sun, M. Pan, F. Tian, X. Li, M. Ye, X. Deng, *Nat. Commun.* **2022**, *13*, 4805.
[40] P. Yao, Z. Chen, T. Liu, X. Liao, Z. Yang, J. Li, Y. Jiang, N. Xu, W. Li, B. Zhu, J. Zhu, *Adv. Mater.* **2022**, 2208236.
[41] D. Li, X. Liu, W. Li, Z. Lin, B. Zhu, Z. Li, J. Li, B. Li, S. Fan, J. Xie, J. Zhu, *Nat. Nanotechnol.* **2021**, *16*, 153.
[42] R. Li, Y. Shi, M. Wu, S. Hong, P. Wang, *Nat. Sustain.* **2020**, *3*, 636.
[43] S. Kim, J. H. Park, J. W. Lee, Y. Kim, Y. T. Kang, *Nat. Commun.* **2023**, *14*, 2374.
[44] G. Wang, Y. Li, H. Qiu, H. Yan, Y. Zhou, *Droplet* **2023**, *2*, e32.
[45] L. Xu, D.-W. Sun, Y. Tian, T. Fan, Z. Zhu, *Chem. Eng. J.* **2023**, *457*, 141231.

© 2024 The Authors. Advanced Energy Materials published by Wiley-VCH GmbH

16146840, 2024, 16, Downloaded from https://onlinelibrary.wiley.com/doi/10.1002/aenm.202303470, Wiley Online Library on [15/07/2024]. See the Terms and Conditions (https://onlinelibrary.wiley.com/terms-and-conditions) on Wiley Online Library for rules of use; OA articles are governed by the applicable Creative Commons License

[46] C. Feng, P. Yang, H. Liu, M. Mao, Y. Liu, T. Xue, J. Fu, T. Cheng, X. Hu, H. J. Fan, K. Liu, *Nano Energy* **2021**, *85*, 105971.
[47] J. Li, X. Wang, D. Liang, N. Xu, B. Zhu, W. Li, *Sci. Adv.* **2022**, *8*, eabq0411.
[48] Y. Zhou, W. Sun, Z. Ling, X. Fang, Z. Zhang, *Ind. Eng. Chem. Res.* **2017**, *56*, 14799.
[49] O. A. Adeleke, A. A. A. Latiff, M. R. Saphira, Z. Daud, N. Ismail, A. Ahsan, *Nanotechnology* **2019**, 1.
[50] F. Deng, Z. Chen, C. Wang, C. Xiang, P. Poredoš, R. Wang, *Adv. Sci.* **2022**, 2204724.
[51] H. Kim, S. Yang, S. R. Rao, S. Narayanan, E. A. Kapustin, H. Furukawa, A. S. Umans, O. M. Yaghi, E. N. Wang, *Science* **2017**, *356*, 430.
[52] A. Krajnc, J. Varlec, M. Mazaj, A. Ristić, N. Z. Logar, G. Mali, *Adv. Energy Mater.* **2017**, *7*, 1601815.
[53] N. Hanikel, M. S. Prévot, F. Fathieh, E. A. Kapustin, H. Lyu, H. Wang, N. J. Diercks, T. G. Glover, O. M. Yaghi, *ACS Cent. Sci.* **2019**, *5*, 1699.
[54] P. A. Kallenberger, M. Fröba, *Communications Chemistry* **2018**, *1*, 28.
[55] K. Yang, Y. Shi, M. Wu, W. Wang, Y. Jin, R. Li, M. W. Shahzad, K. C. Ng, P. Wang, *J. Mater. Chem. A* **2020**, *8*, 1887.
[56] X. Zhang, J. Yang, R. Borayek, H. Qu, D. K. Nandakumar, Q. Zhang, J. Ding, S. C. Tan, *Nano Energy* **2020**, *75*, 104873.
[57] K. Matsumoto, N. Sakikawa, T. Miyata, *Nat. Commun.* **2018**, *9*, 2315.
[58] K. Yang, T. Pan, I. Pinnau, Z. Shi, Y. Han, *Nano Energy* **2020**, *78*, 105326.
[59] R. Li, M. Wu, S. Hong, P. Wang, *Nano Energy* **2020**, *67*, 104255.
[60] H. L. Nguyen, N. Hanikel, S. J. Lyle, C. Zhu, D. M. Proserpio, O. M. Yaghi, *J. Am. Chem. Soc.* **2020**, *142*, 2218.
[61] S. M. Towsif Abtab, D. Alezi, P. M. Bhatt, A. Shkurenko, Y. Belmabkhout, H. Aggarwal, L. J. Weselinski, N. Alsadun, U. Samin, M. N. Hedhili, M. Eddaoudi, *Chem* **2018**, *4*, 94.
[62] A. Karmakar, P. G. M. Mileo, I. Bok, S. B. Peh, J. Zhang, H. Yuan, G. Maurin, D. Zhao, *Angew. Chem., Int. Ed.* **2020**, *59*, 11003.
[63] J. Wang, R. Wang, L. Wang, *Appl. Therm. Eng.* **2016**, *100*, 893.
[64] R. Li, Y. Shi, M. Alsaedi, M. Wu, L. Shi, P. Wang, *Environ. Sci. Technol.* **2018**, *52*, 11367.
[65] Heatwaves and F. S. Europe, NASA earth observatory, Africa, and Asia **2022**.

© 2024 The Authors. Advanced Energy Materials published by Wiley-VCH GmbH

16146840, 2024, 16, Downloaded from https://onlinelibrary.wiley.com/doi/10.1002/aenm.202303470, Wiley Online Library on [15/07/2024]. See the Terms and Conditions (https://onlinelibrary.wiley.com/terms-and-conditions) on Wiley Online Library for rules of use; OA articles are governed by the applicable Creative Commons License